PHYSICAL REVIEW B VOLUME 62, NUMBER 3 15 JULY 2000-I

Emission spectrum of a dipole in a semi-infinite periodic dielectric structure: Effect of the boundary

A. G. Galstyan, M. E. Raikh, and Z. V. Vardeny
Department of Physics, University of Utah, Salt Lake City, Utah 84112
(Received 4 January 2000)

The emission spectrum of a dipole embedded in a semi-infinite photonic crystal is calculated. For simplicity we study the case in which the dielectric function is sinusoidally modulated only along the direction perpendicular to the boundary surface plane. In addition to oscillations of the emission rate with the distance of the dipole from the interface, we also observed that the shape of the emission spectrum srongly depends on the *initial phase* of the dielectric modulation. When the direction of light propagation inside the periodic structure is not normal to the boundary surface plane, we observed aditional singularities in the emission spectrum, which arise due to different angle dependence of the Bragg stop band for TE and TM polarizations.

I. INTRODUCTION

It is well known that the fluorescence lifiteme of an atom can be drastically changed when placed in an inhomogenous medium. In his pioneering work Purcell[1] predicted a strong enhancement of the radiative decay rate of an emitter placed inside a resonant microcavity. In contrast, it was also suggested[2] that spontaneous emission can be totally inhibited if the emitter transition frequency lies below that of the fundamental resonator mode. This effect can be understood in terms of redistribution of photonic density-of-states (DOS) caused by inhomogeneity and/or nontrivial boundary conditions imposed on the radiative field. During the years the spontaneous emission of a dipole coupled to various optical enviroments such as metallic cavities,[3] Fabry-Perot two-mirror cavities,[4] dielectric microspheres,[5] and nanobubbles,[6] has been a subject of extensive theoretical and experimental studies.[7]

Recently there has been a growing interest in studies of radiative properties of fluorescent molecules inside periodic dielectric structures, the so-called photonic crystals (PC).[8,9] The Bragg diffraction of light that occurs in these systems opens up a spectral gap[10] (or a pseudogap) in the photonic DOS in analogy with electronic energy gaps in semiconductors. A quantum electrodynamical approach for the radiative decay inside PC has revealed physical phenomena such as strong suppression of spontaneous emission within the gap and the formation of photon-atom bound states,[11–14] with the localization of superradiant modes near the band edges,[15] etc. Calculations of emission spectra within the framework of classical theory were performed for a one-dimensional Kronig-Penny-type model[16] as well as for three-dimensional fcc lattice structures.[17] It has been established that inhibition of spontaneous emission within the gap is accompanied with strong enhancement at the band edges.[16,17] It was also shown that the emission spectrum strongly depends on the position of the emiter within the unit cell,[16,17] as well as on its orientation.[17] Experimental observations of inhibited spontaneous emission have been reported for different periodic structures.[18–23]

So far, the exsisting theoretical studies have considered infinite periodic structures. As a result, the emission power was identically zero within the gap.[16,17] In the experiments,[18–23] however, the photonic gap appears as a drop by a factor of ~ 2 in the emission power within a certain spectral interval. This points at the important role of the boundary between the photonic crystal and the air, which is studied in the present paper. As we will show below, accounting for a nearby interface results in a nontrivial dependence of the emission spectrum on the *initial phase* of the dielectric modulation. If the distance of the dipole from the boundary surface plane and the dielectric modulation period are, respectively, d and a, then one might expect that the dependence of the emission spectrum on the *initial phase* be small in the parameter a/d. On the contrary, we found that the strong dependence of the emission spectrum on the *initial phase* persists even in the limit $d/a \to \infty$ (provided there is no absorption in the system). We illustrate this effect in the frame of the simplest possible model. Namely, we choose the dielectric modulation to be (i) weak, (ii) one-dimensional, and (iii) sinusoidal. To quantitavely study the effect of a plane boundary we generalize the standard calculations of the emission rate in periodic media for the case of semi-infinite geometry (Sec. II). In Sec. III we present numerical results for emission spectra illustrating the role of the *initial phase*. Discussion of our results and their relevance to recent measurements is presented in Sec. IV.

II. DERIVATION OF THE POWER EMISSION SPECTRUM

We schematically depict the system under consideration in Fig. 1. The dielectric function for the left half-space is constant and equals ε_0, whereas for $x>0$ is given by

$$\varepsilon(x)=\varepsilon_1+\delta\varepsilon\cos(\sigma x+\phi), \tag{1}$$

where ϕ is the initial phase of the dielectric modulation, $\sigma=2\pi/a$ is the modulation wave vector, and $\delta\varepsilon$ is the amplitude of the modulation. Below we assume $\delta\varepsilon \ll \varepsilon_1$. The wave equations for the electric and magnetic fields are

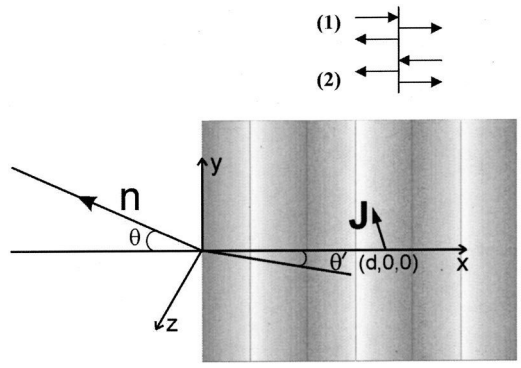

FIG. 1. Schematic representation of our PC system. The emitter is located on the x axis at a distance d from the interface. The unit vector $\mathbf{n}$ lies in the xy plane. Inset: Illustration of two linearly independent solutions of the homogenous equations discussed in the text.

$$\nabla^2\mathbf{E}(\mathbf{r})-\nabla[\nabla\mathbf{E}(\mathbf{r})]+\frac{\omega^2}{c^2}\varepsilon(x)\mathbf{E}(\mathbf{r})=i\frac{4\pi\omega}{c^2}\mathbf{J}(\mathbf{r}), \quad (2)$$

$$\nabla^2\mathbf{B}(\mathbf{r})-\nabla[\ln\varepsilon(x)]\times\nabla\times\mathbf{B}(\mathbf{r})+\frac{\omega^2}{c^2}\varepsilon(x)\mathbf{B}(\mathbf{r}) = -\frac{4\pi}{c}\nabla\times\mathbf{J}(\mathbf{r}), \quad (3)$$

where the radiation source $\mathbf{J}(\mathbf{r})=\mathbf{j}\delta(\mathbf{r}-\mathbf{r}_0)$ is located at point $\mathbf{r}_0=(d,0,0)$. We note that the term proportional to $\delta\varepsilon$ has been neglected in the right-hand sides of Eq. (3). The time averaged radiative power per unit solid angle is given by

$$\frac{dP}{d\Omega}=\frac{c}{8\pi}\mathrm{Re}[r^2\mathbf{n}(\mathbf{E}\times\mathbf{B}^*)], \quad (4)$$

where B^* is the complex conjugate of B, $r=|\mathbf{r}|$, and $\mathbf{n}=\mathbf{r}/r$ is the unit radius vector. Without any loss of generality we choose $n_z=0$ (see Fig. 1). Then it is very convenient to separately treat two possible orientations of the dipole. Indeed, one can easily check that the current density components J_z and J_x,J_y give rise to electro-magnetic (EM) radiation with, respectively, electric (TE polarization) and magnetic (TM polarization) fields polarized in the z direction. Since these two modes do not interfere, their contributions to the radiation power are additive. The corresponding EM wave equations for the two polarizations are obtained from the z components of Eqs. (2) and (3) by taking the Fourier transform with respect to the y and z coordinates:

$$\frac{d^2E_z}{dx^2}+\left(\frac{\omega^2}{c^2}\varepsilon(x)-k_y^2\right)E_z=\frac{4\pi i\omega}{c^2}j_z\delta(x-d) \quad (\mathrm{TE}), \quad (5)$$

$$\frac{d^2B_z}{dx^2}-\left(\frac{\partial\ln\varepsilon}{\partial x}\right)\frac{dB_z}{dx}+\left(\frac{\omega^2}{c^2}\varepsilon(x)-k_y^2\right)B_z = -\frac{4\pi}{c}\left(\frac{\partial j_y}{\partial x}-ik_yj_x\right)\delta(x-d) \quad (\mathrm{TM}), \quad (6)$$

where k_y is the y component of the wave vector $[E_z(x;k_y),B_z(x;k_y)\propto e^{ik_yy}]$. Since we want to calculate the power emmited in the xy plane, we have set $k_z=0$ in Eqs. (5) and (6). The solution of the corresponding homogenous equations may be written as a sum of incident, reflected, and transmitted EM waves, with two linearly independent terms $E_1(x)$, $E_2(x)$ and $B_1(x)$, $B_2(x)$ corresponding to the incident EM wave from the right and left, respectively (see inset of Fig. 1). To solve Eqs. (5) and (6) we employ the variation of a constant method. We seek solution in the form:

$$E_z(x)=C_1^E(x)E_1(x)+C_2^E(x)E_2(x),$$

$$B_z(x)=C_1^B(x)B_1(x)+C_2^B(x)B_2(x). \quad (7)$$

Upon substituting Eq. (7) into Eqs. (5) and (6) we find for the variational coefficients

$$C_{1,2}^E(x)=i\omega\frac{4\pi}{c^2}W_E^{-1}\int_{X_{1,2}^E}^{x}dx'\,E_{2,1}(x')j_z\delta(x'-d), \quad (8)$$

$$C_{1,2}^B(x)=-\frac{4\pi}{c}W_B^{-1}\int_{X_{1,2}^B}^{x}dx'\,B_{2,1}(x')\times\left(\frac{\partial j_y}{\partial x'}-ik_yj_x\right)\delta(x'-d), \quad (9)$$

where W_E, W_B are the Wronskians

$$W_E=E_1\frac{dE_2}{dx}-E_2\frac{dE_1}{dx}, \quad W_B=B_1\frac{dB_2}{dx}-B_2\frac{dB_1}{dx} \quad (10)$$

and $X_{1,2}^E$, $X_{1,2}^B$ in the lower integration limits are constants of integration. They are determined from the boundary conditions that there are no incoming EM waves, implying $X_1^E=X_1^B=\infty$, $X_2^E=X_2^B=-\infty$. Hence, the solutions of Eqs. (5) and (6) for large negative x, which satisfy the boundary conditions, can be written as follows:

$$E_z(x)=i\omega\frac{4\pi}{c^2}W_E^{-1}j_zE_1(d)E_2(x), \quad (11)$$

$$B_z(x)=\frac{4\pi}{c}W_B^{-1}\left(j_y\left.\frac{dB_1}{dx}\right|_{x=d}+ik_yj_xB_1(d)\right)B_2(x). \quad (12)$$

It can be easily shown that for negative x one has $W_E^{-1}E_2(x)=W_B^{-1}B_2(x)=ie^{-ik_xx}/2k_x$. Thus, the remaining task is to find $E_1(d)$, $B_1(d)$, and $(dB_1/dx)_{x=d}$.

The solution of the homogeneous equations for the left half-space can be written as a sum of two plane waves,

$$E_1(x)=e^{-ik_xx}+R_Ee^{ik_xx}, \quad B_1(x)=e^{-ik_xx}+R_Be^{ik_xx}, \quad (13)$$

where R_E, R_B are the optical reflection coefficients for TE and TM polarizations, respectively. For the right half-space one may use the Bloch theorem to find the solution

$$E_1(x)=e^{iq_Ex}\sum_{n=-\infty}^{\infty}A_n^Ee^{i\sigma nx}, \quad B_1(x)=e^{iq_Bx}\sum_{n=-\infty}^{\infty}A_n^Be^{i\sigma nx}. \quad (14)$$

When substituting Eq. (14) into Eqs. (5) and (6) we obtain two infinite systems of linear, homogenous equations for the coefficents A_n^E, A_n^B:

$$\left(\frac{\omega^2}{c^2}\varepsilon_1 - k_y^2 - (q_E + n\sigma)^2\right)A_n^E + \frac{\omega^2}{c^2}\frac{\delta\varepsilon}{2}(e^{i\phi}A_{n-1}^E + e^{-i\phi}A_{n+1}^E) = 0, \tag{15}$$

$$\left(\frac{\omega^2}{c^2}\varepsilon_1 - k_y^2 - (q_B + n\sigma)^2\right)A_n^B + \frac{\delta\varepsilon}{2\varepsilon_1}e^{i\phi}\left(\frac{\omega^2}{c^2}\varepsilon_1 + \sigma[q_B + (n-1)\sigma]\right)A_{n-1}^B + \frac{\delta\varepsilon}{2\varepsilon_1}e^{-i\phi}\left(\frac{\omega^2}{c^2}\varepsilon_1 - \sigma[q_B + (n+1)\sigma]\right)A_{n+1}^B = 0. \tag{16}$$

We note that the *initial phase* ϕ explicitly enters into these equations.

Near the Bragg resonance that occurs at $q_{E,B} \approx \sigma/2$, the main coefficents that contribute to the sums in Eq. (14) are A_0^E, A_0^B and A_{-1}^E, A_{-1}^B since the rest of $A_n^{E,B}$ are small in the parameter $\delta\varepsilon/\varepsilon_1$. In this approximation the equation systems (15) and (16) may be simplified into two 2×2 matrix equations. Requiring the determinants of these matrices to vanish, one finds the dispersion relations for the two EM polarizations near resonance

$$\delta q_E = \frac{\sigma}{2\kappa}\sqrt{\left(\frac{\delta\omega}{\omega_0}\right)^2 - \Delta^2}, \tag{17}$$

$$\delta q_B = \frac{\sigma}{2\kappa}\sqrt{\left(\frac{\delta\omega}{\omega_0}\right)^2 - \Delta^2(1-2\kappa)^2}, \tag{18}$$

where we have introduced $\Delta = \delta\varepsilon/4\varepsilon_1$, $q_{E,B} - \sigma/2 = \delta q_{E,B} \ll \sigma/2$, $\omega - \omega_0 = \delta\omega \ll \omega_0$, $\kappa = \sigma^2 c^2/4\omega_0^2\epsilon_1$, and the k_y-dependent resonant frequency ω_0 is given by

$$\omega_0 = \frac{c}{\varepsilon_1}\sqrt{\sigma^2/4 + k_y^2}. \tag{19}$$

Equations (17) and (18) show that there is a spectral gap for EM waves propagating in the system centered at ω_0. For both TE and TM polarizations the central gap position shifts to higher frequencies with increasing k_y (which also determines the propagation direction of the radiative field). For TE polarization the gap broadens with increasing angle θ' (see Fig. 1) whereas for TM polarization the gap narrows and disappears at $2\kappa = 1$, which corresponds to the propagation direction for which $k_y = \sigma/2$. This can be defined as a Brewster angle for Bragg diffraction. If one increases k_y further, then the gap reopens again.

Using Eqs. (15)–(18) we obtain the following expressions for the electric and magnetic fields for the right-half space:

$$E_1(x) = A_{-1}^E e^{i\delta q_E x}(e^{i\sigma x/2} - F_E e^{-i\phi}e^{-i\sigma x/2}), \tag{20}$$

$$B_1(x) = A_{-1}^B e^{i\delta q_B x}(e^{i\sigma x/2} - F_B e^{-i\phi}e^{-i\sigma x/2}). \tag{21}$$

Here the functions F_E and F_B describe the coupling between incident and Bragg reflected waves and are defined as follows:

$$F_E(\delta\omega,\theta) = \frac{1}{\Delta}\left(\frac{\delta\omega}{\omega_0} - \sqrt{\left(\frac{\delta\omega}{\omega_0}\right)^2 - \Delta^2}\right), \tag{22}$$

$$F_B(\delta\omega,\theta) = \frac{1}{\Delta(1-2\kappa)}\left(\frac{\delta\omega}{\omega_0} - \sqrt{\left(\frac{\delta\omega}{\omega_0}\right)^2 - \Delta^2(1-2\kappa)^2}\right). \tag{23}$$

Finally, we match the fields components and their derivatives at $x = 0$, take the inverse Fourier transform with respect to k_y, k_z, and use Eq. (4) to get the following expression for the total radiated power $dP/d\Omega$, normalized to the radiation power when there is no dielectric modulation:

$$\left(\frac{dP}{d\Omega}\right)_N = \frac{j_z^2 T_{0E}^2}{j_z^2 T_{0E}^2 + \varepsilon_1 j_1^2 T_{0B}^2}\left|\frac{1 - F_E e^{-i(\sigma d + \phi)}}{1 - R_{0E}F_E e^{-i\phi}}e^{i\delta q_E d}\right|^2 + \frac{\varepsilon_1 j_1^2 T_{0B}^2}{j_1^2 T_{0E}^2 + \varepsilon_1 j_1^2 T_{0B}^2}\left|\frac{1 - \chi F_B e^{-i(\sigma d + \phi)}}{1 - R_{0B}F_B e^{-i\phi}}e^{i\delta q_B d}\right|^2. \tag{24}$$

Here T_{0E}, R_{0E} and T_{0B}, R_{0B} are the conventional Fresnel's transmission and reflection coefficients from the dielectric interface without the dielectric modulation for the amplitudes of TE and TM polarized waves, respectively, $j_1 = j_y\cos\theta' + j_x\sin\theta'$, where θ' is related to the observation angle θ by Snell's law. The quantity χ, which depends on the dipole orientation in the xy plane, is defined as $\chi = (j_y - j_x\tan\theta')/(j_y + j_x\tan\theta')$.

Equation (24) is the main result of this paper. We note that the phase ϕ is explicitly present in both the numerator and denominator of Eq. (24), indicating the important role of the *initial modulation phase* at the boundary interface. In the next section we numerically analyze the role of ϕ in the emission spectrum for different situations.

III. NUMERICAL RESULTS

Before presenting our numerical results let us concentrate on a particular experimental case of opals[21,22] and opal replica.[22] These artificial photonic crystals consist of closely packed SiO_2 spheres forming an fcc structure that contains fully interconnected voids. The opal replica is formed by filling these voids with a precursor polymer solution and then etching the SiO_2 spheres after polymerization.[22] The opals and opal replica PC are infiltrated with various fluorescent dye solutions to provide a radiation source inside the crystal. Inhibited spontaneous emission of the dye molecules in such PC have been recently studied by several groups.[21,22] The refractive index n of SiO_2 is $n \approx 1.46$ and the refractive index contrast Δn between the SiO_2 balls and the dye solution ranges between $\Delta n \approx 0.1 - 0.3$. This is not sufficient for a formation of a *complete* photonic band gap. Instead, the system posseses pseudogaps (or partial gaps) with an angle-dependent central frequency. To compare our results to the

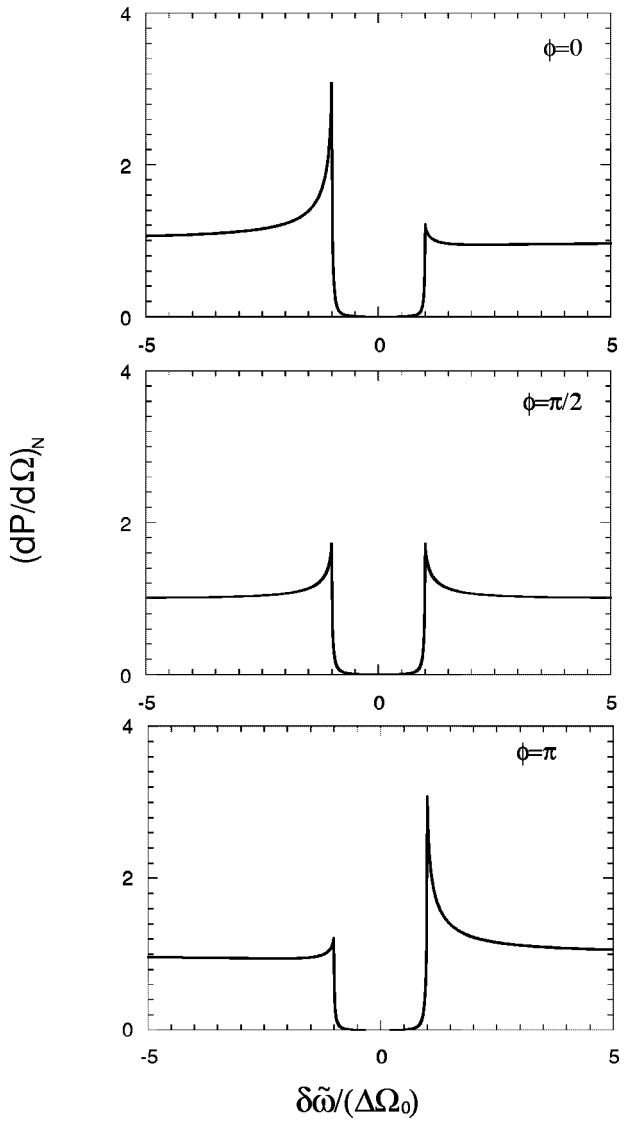

FIG. 2. Normalized emission power $(dP/d\Omega)_N$ averaged over the dipole emitter orientations at $\theta=0$ for $\phi=0,\pi/2$ and π. Here $\delta\tilde{\omega}=\omega-\Omega_0$ is the deviation from the Bragg frequency at $\theta=0$. Calculations were performed with $\varepsilon_1=3\varepsilon_0=3$ and $\Delta=0.1$. The emitter is five periods away from the interface $(d=5a)$ implying strong suppression of the emission within the gap.

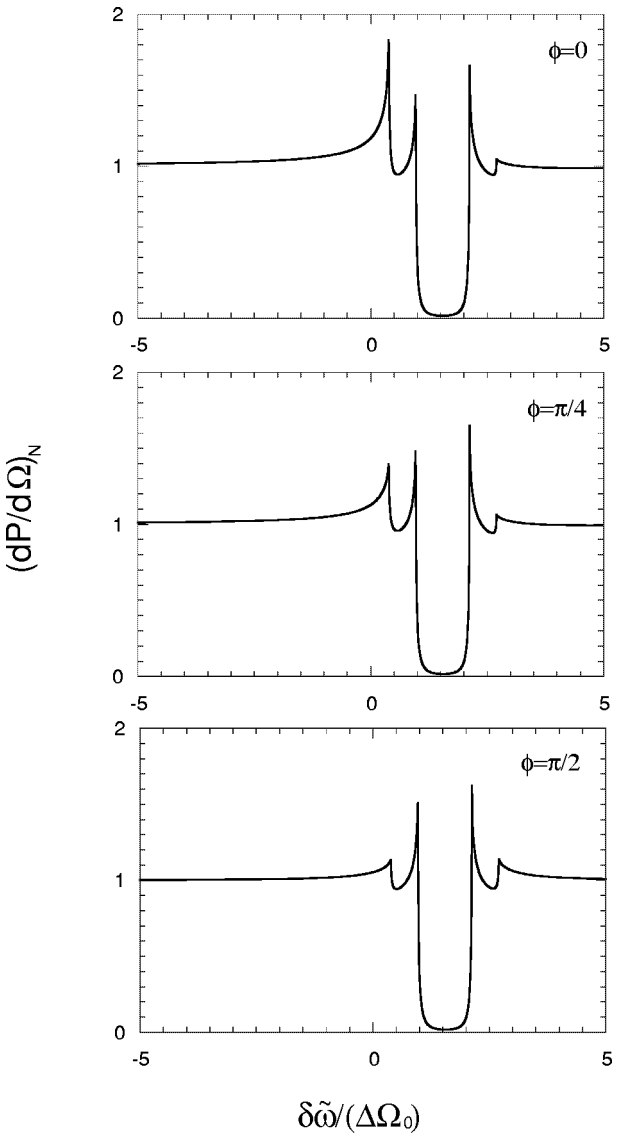

FIG. 3. Normalized and averaged power emission $(dP/d\Omega)_N$ at $\theta=60°$ for $\phi=0,\pi/4$, and $\pi/2$. The rest of the parameters are the same as in Fig. 2.

experiments we have chosen in our model $\Delta=\delta\varepsilon/4\varepsilon_1=0.1$.

First, we consider the case when the emitter is many periods away from the interface $(d=5a)$.[24] In Fig. 2 we show the emission power *averaged* over the orientations of the emitter *as well as over its position* within the unit cell [the zero on the frequency axis in all plots corresponds to the central gap frequency Ω_0 at $\theta=0$, where $\Omega_0=\sigma c/(2\sqrt{\varepsilon_1})$]. Inside the gap, the emission power is strongly suppressed. It is seen, however, that even in the limit of large d/a the features of the *averaged* emission power still depend on the *initial phase*.

The evolution of $(dP/d\Omega)_N$ with ϕ outside the gap is described as follows. At $\phi=0$ there is a well-pronounced singularity at the lower edge of the spectral gap. With increasing ϕ, this singularity diminishes whereas another singularity starts to develop at the upper edge; the spectrum becomes symmetric at $\phi=\pi/2$. Further increase of ϕ leads to a gradual transformation of the initial curve into its mirror image with respect to the central gap frequency, the singularity now occuring at the upper band edge.

Figure 2 corresponds to $\theta=0$. The sensitivity of the emission power to ϕ appears to be even more pronounced for $\theta\neq0$. We illustrate this effect by plotting in Fig. 3 the *averaged* $(dP/d\Omega)_N$ for $\theta=60°$ for the set of *initial phases* $\phi=0,\pi/4,\pi/2$. With increasing ϕ again, it is seen that there is a tendency for the emission spectrum to become symmetric near $\phi=\pi/2$. At $\phi=\pi$ (not presented here) the emission spectrum is again transformed into the mirror image of the initial curve at $\phi=0$ but now with respect to the shifted central gap frequency $\Omega_0/\cos\theta'$. We also note the appearance of additional singularities in the emission spectrum. Their origin lies in the different angle dependencies of the gap width for TE and TM polarizations, as seen before in Eqs. (17) and (18). To be more specific, we note that the highest-and lowest-frequency peaks correspond to the band edges for TE polarization. Similarly, two peaks at the intermediate frequencies determine the band edges for TM polar-

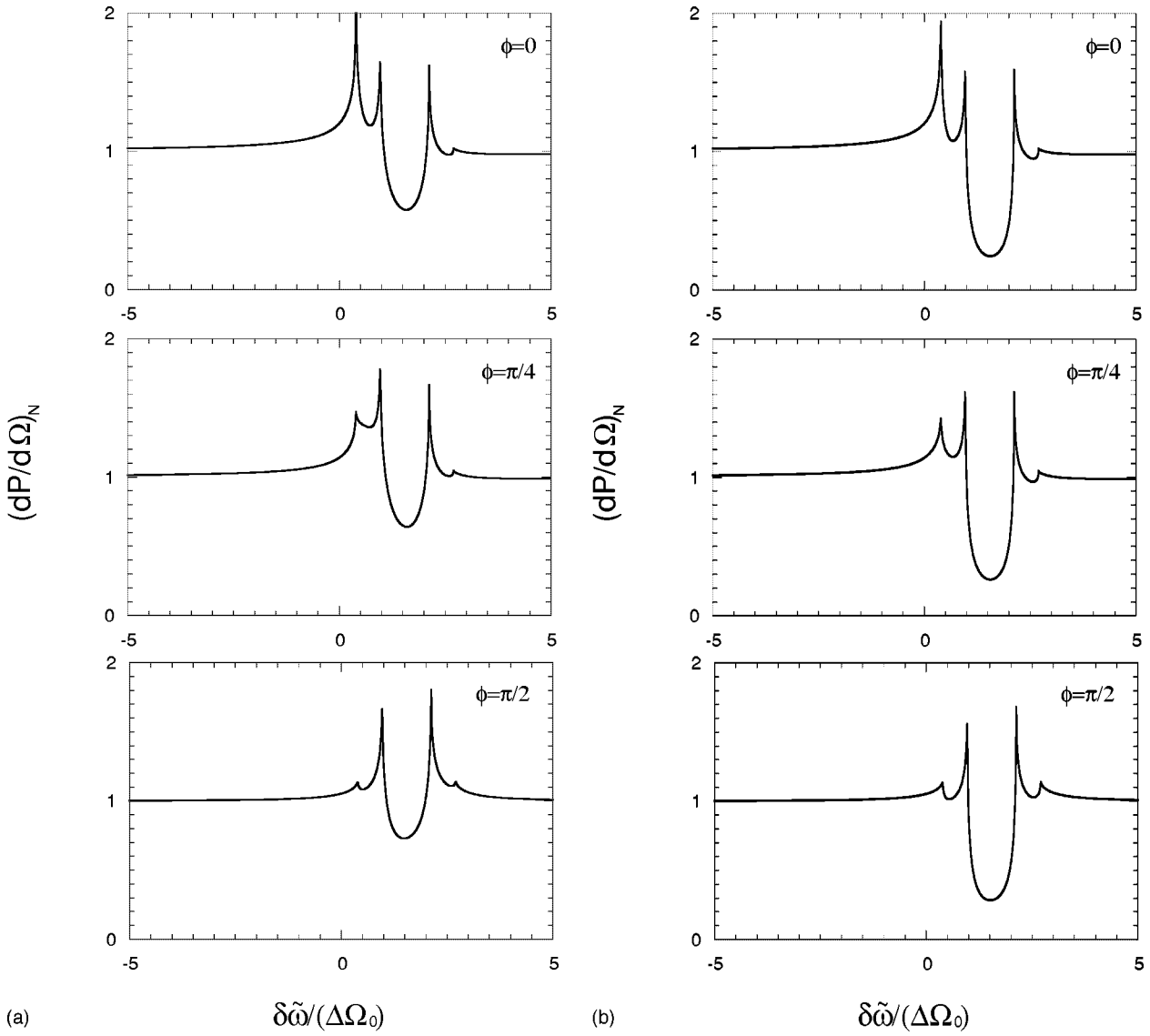

FIG. 4. Emission spectrum of the emitter located at (a) $N=1$, (b) $N=2$ periods away from the boundary for $\theta=60°$ and for the same set of the initial phases as in Fig. 3. Averaging over the position within the unit cell and over all possible orientaions of the dipole emitter direction has been performed.

ization. Both pairs of the singularities are located symetrically around the shifted Bragg frequency $\omega_0=\Omega_0/\cos\theta'$.

Let us now turn to the discussion of the case where the emitter is close to the interface. The main feature of this situation is that $(dP/d\Omega)_N$ *inside* the gap remains finite. One can see from Eq. (24) that moving the emitter N periods away from the boundary decreases the emission power at the center of the gap by a factor of $\exp(-2\pi N\Delta)$. Therefore, to study the features of the spontaneous emission inside the gap, we choose $N=1,2$. This situation is illustrated in Fig. 4 where we plot the averaged $(dP/d\Omega)_N$ for the observation angle $\theta=60°$. One can see that the evolution of the emission power by increasing the *initial phase* is very strong. Again, we note that there are four well-pronounced singularities in the emission spectrum that correspond to the spectral gap edges of the TE and TM polarizations. In particular, for $\phi=0$ there is a noticable enhancement of the emission rate (by a factor of ~ 2) at the frequency that determines the lower band edge of the TE polarization, whereas for $\phi=\pi/2$ a similar enhancement occurs at the edges of the TM polarization gap.

Finally, in Fig. 5 we plot the emission power integrated over the observation angle θ (i.e., the total power emitter in the xy plane) for $\phi=0$ and $\phi=\pi$. In this case too, an averaging over the dipole position within the unit cell has been performed. To allow for an unpolarized emission we have chosen $j_x=j_y=j_z$. Remarkably, even after angular averaging a weak dependence of the emission power on the initial phase still persists.

IV. DISCUSSION

We have studied the emission spectrum of a dipole inside a one-dimensional periodic structure in the presence of a nearby plane boundary. As expected, the emission rates are strongly suppressed for frequencies inside the spectral gap, provided that the emitter is many periods away from the interface $(d/a>5)$. For frequencies near the band edges, the

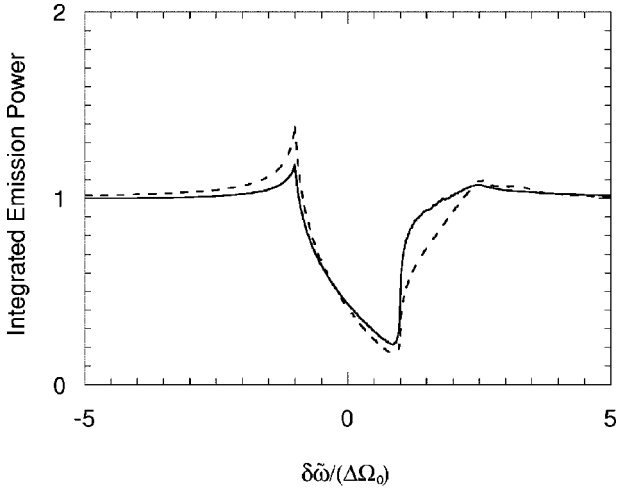

FIG. 5. The total power emitted in the xy plane for $\phi=0$ (solid line) and $\phi=\pi$ (dashed line). Here $j_x=j_y=j_z$, $d=2a$. Averaging over the dipole emitter position within the unit cell has been performed.

emission spectrum changes drastically with the *initial phase* of the dielectric modulation. We also observed enhancement of the emission rates near the band edges, however, by a factor much smaller than predicted in the previous studies.[16,17] This can be attributed to the fact that the modulation in our model is weak. In Ref. 17, where the total radiation power from a dipole inside a infinite 3D fcc lattice was calculated numerically, the contrast in the dielectric constant $\Delta\varepsilon$ was more than 10 allowing for the formation of a complete photonic band gap. This resulted in an enhancement of the radiated power at the band edges by a factor of ~ 25. Similarly, in Ref. 16, where the authors considered a 1D Kronig-Penney-type modulation of the refractive index, the enhancement factor at the band edges was about ~ 30, whereas inside the gap it was identically zero. Apparently, this resulted from consideration of radiative modes polarized parallel to the dipole direction. Allowing for nonpolarized radiation (i.e., in all directions) should lead to qualitatively different results (see, for example, Fig. 5). Strictly speaking, the straightforward comparision of our calculation with those of previous studies is not possible due to the different approach developed here. However, it is clear from our consideration that the sensitivity of the power emission to the boundary conditions should persist also for strong and non-sinusoidal modulation and become even stronger.

In this paper we also studied the case where the emitter is sufficiently close to the interface, so that the emission power for the frequencies inside the gap is finite. In this case also we showed that the features of the emission spectrum are very sensitive to the initial phase of the periodic modulation, hence emphasizing the effect of the boundary.

We note that in our calculations we assumed that no deffects exist in the system. In the presence of weak disorder the emission spectrum would be significantly modified. Let us consider radiation from a dipole that is many periods away from the boundary with a frequency inside the spectral gap. If there are no defects then the radiation (e.g., in the direction normal to the boundary) is strongly attenuated (see Fig. 2). However, introducing a small concentration of defects opens up a new mechanism for the light emission to come out from the PC in the direction *normal* to the boundary. Namely, light can propagate without any attenuation in directions for which the Bragg condition is not satisfied and then scatter off defects that are close to the interface. As a result, the emission power in the direction normal to the boundary is not exponentially small but is finite, similar to the case of a dipole close to the boundary. Remarkably, only defects close to the boundary, within the Bragg attenuation length $\xi_B=(2\pi\sigma\Delta)^{-1}$ from the interface, contribute to the emission power. Owing to this effect, we conclude that the emission spectrum in the presence of a weak disorder is rather universal, since it does not depend on the dipole-interface distance d. Experimentally this was demonstrated in Ref. 23, where the authors found a way to excite fluorescent dye molecules at different distances from the boundary. They have demonstrated that the emission power at the center of the spectral gap is attenuated by a factor of ~ 2 and does not change upon changing d. This was interpretated in terms of light scattering off defects close to the PC interface.

ACKNOWLEDGMENTS

The authors thank N. Eradat, Dr. A. A. Zakhidov, and Dr. R. H. Baughman for useful discussions. This work was supported in part by NSF under Grant No. DMR–9732820 and the International Research Foundation of NEDO (Japan). One of the authors (M. E. R.) acknowledges the support of the Petroleum Research Fund under Grant No. ACS–PRF No. 34302–AC6.

[1] E.M. Purcell, Phys. Rev. **69**, 681 (1946).
[2] D. Kleppner, Phys. Rev. Lett. **47**, 233 (1981).
[3] P. Goy, J.M. Raimond, M. Gross, and S. Haroche, Phys. Rev. Lett. **50**, 1903 (1983); W. Jhe, A. Anderson, E.A. Hinds, D. Meschede, and L. Moi, *ibid.* **58**, 666 (1987); D.J. Heinzen, J.J. Childs, J.E. Thomas, and M.S. Feld, *ibid.* **58**, 1320 (1987).
[4] R.R. Chance, A.H. Miller, A. Prock, and R. Silbey, J. Chem. Phys. **63**, 1589 (1975).
[5] H. Chew, Phys. Rev. A **38**, 3410 (1988).
[6] V.V. Klimov and V.S. Letokhov, Chem. Phys. Lett. **301**, 441 (1999).
[7] S. Haroche and D. Kleppner, Phys. Today **42**, 24 (1989).
[8] E. Yablonovitch, Phys. Rev. Lett. **58**, 2059 (1987).
[9] S. John, Phys. Rev. Lett. **58**, 2486 (1987).
[10] For a review see *Photonic Bandgaps and Localization*, edited by C. M. Soukoulis (Plenum Press, New York, 1993).
[11] S. John and J. Wang, Phys. Rev. B **43**, 12 772 (1991).
[12] S. John and T. Quang, Phys. Rev. A **50**, 1764 (1994).
[13] V.I. Rupasov and M. Singh, Phys. Lett. A **222**, 258 (1996).
[14] S. John and J. Wang, Phys. Rev. Lett. **64**, 2418 (1990).
[15] S. John and T. Quang, Phys. Rev. Lett. **74**, 3419 (1995).
[16] J.P. Dowling and C.M. Bowden, Phys. Rev. A **46**, 612 (1992).
[17] T. Suzuki and P.K.L. Yu, J. Opt. Soc. Am. B **12**, 570 (1995).
[18] J. Martorell and N.M. Lawandy, Phys. Rev. Lett. **65**, 1877 (1990).
[19] B.Y. Tong, P.K. John, Y.-t Zhu, Y.S. Liu, S.K. Wong, and W.R. Ware, J. Opt. Soc. Am. B **10**, 356 (1993).
[20] T. Yamasaki and T. Tsutsui, Appl. Phys. Lett. **72**, 1957 (1998).

[21] E.P. Petrov, V.N. Bogomolov, I.I. Kalosha, and S.V. Gaponenko, Phys. Rev. Lett. **81**, 77 (1998); M. Megens, H.P. Schriemer, A. Lagendijk, and W.L. Vos, *ibid.* **83**, 5401 (1999).
[22] K. Yoshino, S.B. Lee, S. Tatsuhara, Y. Kawagishi, M. Ozaki, and A.A. Zakhidov, Appl. Phys. Lett. **73**, 3506 (1998).
[23] M. Megens, J.E.G.J. Wijnhoven, A. Lagendijk, and W.L. Vos, J. Opt. Soc. Am. B **16**, 1403 (1999).
[24] Plotting Eq. (24) for different emitter-interface distances d we realized that $d=5a$ differs only weakly from $d=\infty$, in the sense, that the typical value of the power intensity within the gap amounts to less than 5% of its value outside the gap.